ID-1069

AN EXPERIMENTAL AND NUMERICAL INVESTIGATION INTO THE FAILURE OF COMPRESSIVELY LOADED STIFFENER RUNOUT SECTIONS

Brian G. Falzon and G. A. O. Davies

Department of Aeronautics, Imperial College of Science, Technology and Medicine, Prince Consort Road, London, SW7 2BY, U.K.

SUMMARY

Recent efforts towards the development of the next generation of large civil and military transport aircraft within the European community have provided new impetus for investigating the potential use of composite material in the primary structure. One concern in this development is the vulnerability of co-cured stiffened structures to through-thickness stresses at the skin-stiffener interfaces, particularly in stiffener runout regions. These regions are an inevitable consequence of the requirement of terminating stiffeners at cutouts, rib intersections or other structural features which interrupt the stiffener load path. In this respect, thicker-skinned components are more vulnerable than thin-skinned ones.

This work presents an experimental and numerical study of the failure of thick-sectioned stiffener runout specimens loaded in uniaxial compression. The experiments revealed that failure was initiated at the edge of the runout and propagated across the skin-stiffener interface. High compressive and frictional forces at the edge of the runout were also deduced from a fractographic analysis and it is postulated that these forces may enhance the apparent fracture toughness of the specimens. Finite element analysis using an efficient thick-shell element formulation and the Virtual Crack Closure Technique (VCCT) was able to qualitatively predict the crack growth characteristics for each specimen.

KEYWORDS : stiffener runout, failure, crack growth, compression testing.

INTRODUCTION

The recently proposed designs of the next generation of large civil and military transports in Europe incorporate extensive use of advanced composite material in the primary structure, including a composite outer wing section. The use of thick-skinned co-cured or co-bonded stiffened structures, typical of wing box construction, exacerbates the vulnerability of such structures to through-thickness stresses identified in [1-2]. This is of particular concern in regions where stiffeners are terminated at cutouts or other structural features, such as a rib, which interrupt the stiffener load path. As the stiffener is terminated, the loads through it must be transferred to the skin and hence the design of this termination region becomes significant. It is common practice to taper the stiffener to provide partial relief of the high peel and interlaminar shear stresses that develop in this region. The loss in cross-sectional area due to the terminating

stiffener is sometimes compensated for by a corresponding increase in the skin thickness whereby the skin thickness is ramped up as the stiffener is run out.
The failure of a stiffener runout region was shown to be the critical failure mode on the composite centre wing box section of a C-130 transport aircraft [3] which was developed as part of NASA's Advanced Composites Technology (ACT) program. A compression test by Brooks [4], on a co-bonded hat-stiffened runout panel, also showed that failure occurred at 70.5% of the design ultimate load and was due to unstable crack propagation at the skin-stiffener interface.

In this paper, the experimental results of three thick-skinned co-cured stiffener runout specimens loaded in uniaxial compression are presented. In all specimens, failure was shown to occur at the skin-stiffener interface. A fracture mechanics approach, utilising strain energy release rate curves, was adopted in the finite element analysis of these specimens. Particular emphasis was placed on developing efficient analytical methodologies within a finite element analysis context to predict the behaviour of these critical regions.

EXPERIMENTAL PROGRAMME

SPECIMEN PREPARATION

The results of three types of stiffener runout specimens are presented in this paper. These specimens were co-cured and characterised by a tapered blade stiffener mounted on an effective skin section. The sizing of the specimens was such as to ensure that interlaminar shear stress failure occurred within the skin-stiffener interfaces at a loading below the Euler buckling loads. The first specimen, SPEC-1, shown in Fig. 1, had an overall test length of 440 mm and a width of 120 mm. The stiffener length was 400 mm and the blade was tapered linearly over a distance of 200 mm to a height of 10.0 mm above the skin at the edge of the runout. The blade was mounted on 8.0 mm thick skin resulting in a region of unsupported skin of length 40 mm. The second specimen, SPEC-2 (Fig. 2) was similar to SPEC-1 but with a skin thickness which increased linearly from 8.0 mm to 15.0 mm over the tapered length of the stiffener. The third specimen, SPEC-3, had a constant, but thicker, skin thickness of 13.0 mm with corresponding increases in stiffener thickness dimensions as shown in Fig. 3. SPEC-3 had a test length of 540 mm and was 200 mm wide, with an unsupported skin length of 40 mm. The stiffener web was tapered over a distance of 400 mm. The material used for these specimens was a unidirectional carbon-fibre composite AS4/8852 and nominal material properties are given in Table 1. The lay-up details for each specimen are given in Table 2. Figs 1-3 also show the location of strain gauges on each specimen. The bracketed strain gauge numbers refer to those gauges mounted on the outer surface of the specimen (defined as the smooth surface which would form the aerodynamic surface of a wing structure) directly beneath the gauges shown in the diagram.

Table 1 : Nominal Material Properties for AS4/8552 Unidirectional Composite @ 60 V_f, dry.

Property	Value
Longitudinal tensile modulus	135 GPa
Longitudinal compressive modulus	128 GPa
Transverse tensile modulus	9.5 GPa
Transverse compressive modulus	10.3 GPa
In-plane shear modulus	4.9 GPa
Poisson's ratio	0.3
Longitudinal tensile strength	1.68 GPa
Longitudinal compressive strength	1.1 GPa
Transverse tensile strength	61 MPa
Transverse compressive strength	244 MPa

In-plane shear strength	90 GPa
Ply thickness	0.25 mm

Table 2 : Lay-up Details for Specimens[a]

SPEC-1	
Skin	$[45/-45/0/90/0_2/-45/45/0_2/90/0_2/45/-45/0]_S$
Stiffener (per half section)	$[0/90/0_2/-45/45/0_4/-45/45/0_2/90/0_3/90/0]$
Closing plies	$[0/90/0_2]$
SPEC-2	
Skin (thin section)	$[45/-45/90/0_2/45/-45/0_3/45/-45/0/45/0/90]_S$
Skin (thick section)	$[45/-45/90/0/45/-45/0/90/0_3/45/-45/0/45/-45/0_3/45/-45/0_3/45/-45/0/90/0_2]_S$
Stiffener (per half section)	$[0/90/0_2/-45/45/0_4/-45/45/0_2/90/0_3/90/0]$
Closing plies	$[0/90/0_2]$
SPEC-3	
Skin	$[45/-45/0_2/90/0_2/45/-45/0_3/45/-45/0/90/0_2/45/-45/0/90/0_2/45/-45]_S$
Stiffener (per half section)	$[-45/0_2/45/0_2/90/0_2/45/0/90/0_2/90/0/-45/0_2/90/0_2/45/0_2/-45_2/45]$
Closing plies	[-45/45]

[a] The skin and closing plies lay-up are given from the outer to inner surfaces of the specimen with the outer layer defined as the smooth surface which would form part of the aerodynamic surface in a wing structure and the inner surface defined as the surface on which the stiffener is mounted. The lay-up for the half-stiffener is quoted from the bottom flange surface, at the stiffener/closing plies interface, to the free surface.

EXPERIMENTAL RESULTS

SPEC-1

Fig. 1 shows the location of two pairs of back-to-back strain gauges. Fig. 4 shows the strain readings from these gauges. It is noted that very little strain was recorded by SG 2 close to the end of the runout, where the compressive strains are counteracted by the tensile bending strains at this location. The unsupported region deformed such that the inner surface was at a higher compression than the outer surface (as is evident from the SG 1 and SG 2 readings). SG 3 and SG 4, which were mounted on the stiffened region, recorded a higher compressive strain on the outer surface. This curvature can be measured by the differences in SG 1-SG 2 and SG 3-SG 4, so clearly the unsupported region is undergoing large bending deformation. These local changes in curvature arose from the geometric discontinuity at the edge of the stiffener runout. The strain measured at the centre of the stiffener flange and close to the stiffener's edge (SG 3) was significantly lower than that the strain measured by SG 1.

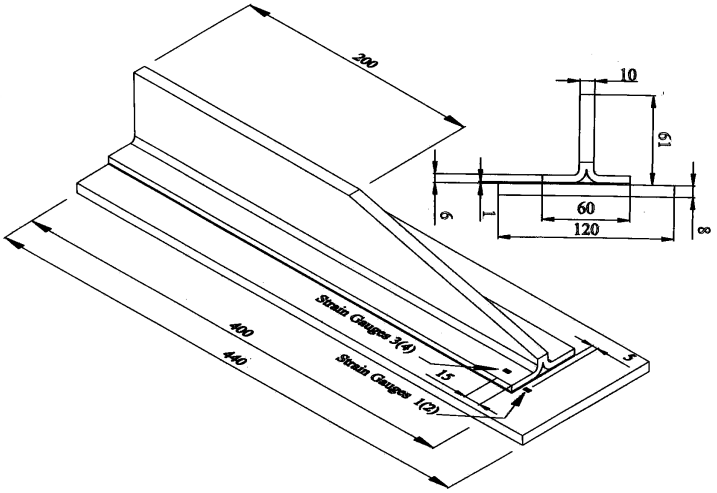

Fig. 1 SPEC-1

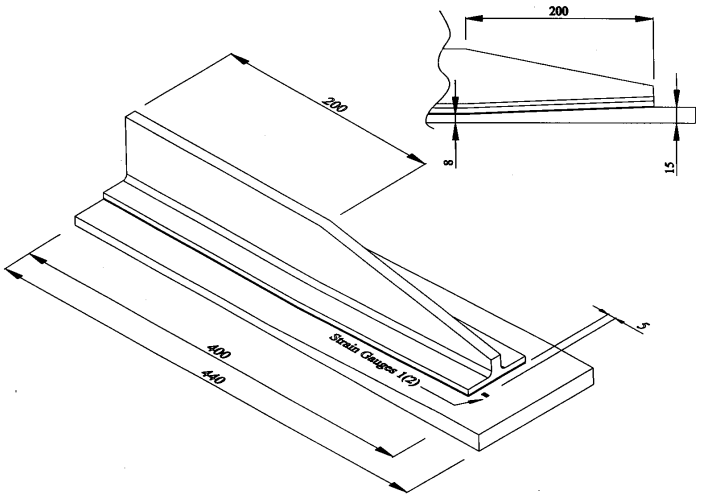

Fig. 2 SPEC-2

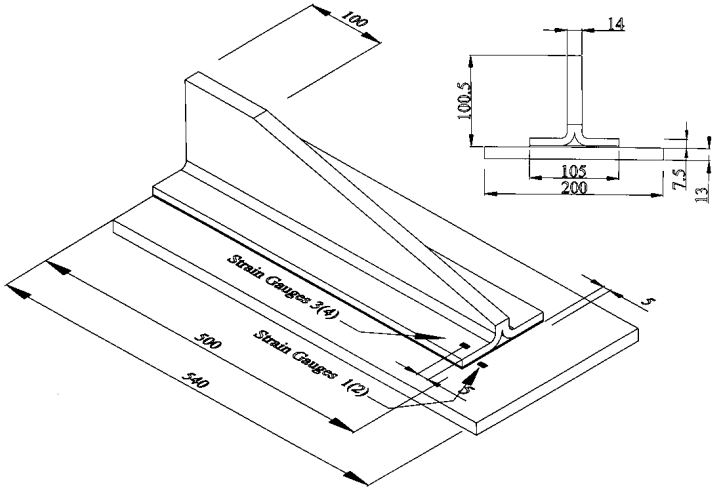

Fig. 3 SPEC-3

The specimen failed catastrophically at a loading of 245 kN at the 0°/90° interface of the closing plies. These plies are located between the top surface of the skin and the base of the stiffener flanges. Crack initiation and propagation was almost instantaneous and highly unstable with the crack propagating across the whole interface. Acoustic emission monitoring recorded a marked increase in activity just before failure although the specimen could not be unloaded in time to arrest crack propagation.

To gain a better understanding of the failure processes in this specimen, a fractographic analysis of the failure surface was undertaken and micrographs used for this analysis are shown in Fig. 5. For clarity, only half the width is shown; examination showed that there was symmetry in the fracture surface morphology across the mid-width. Upon initiation at the tip, the fracture had migrated through the 0° ply in the stiffener, into the 0°/90° ply interface. The morphological

study also revealed that close to the end of the stiffener runout (0.5 mm) there was extensive crushing and fretting across the whole width of the crack front which was indicative of high out-

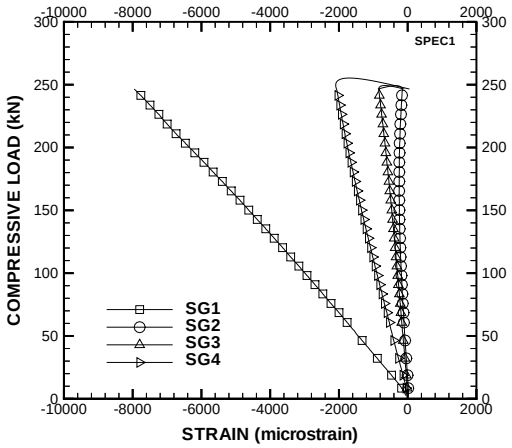

Fig. 4 Strain gauge results for SPEC-1

of-plane compressive forces. These forces arise from the loading offset on the stiffener. At 10 mm away from the edge it was observed that the crushing is greater towards the edges and negligible towards the centre. These high compressive forces may delay the onset of crack initiation and the analytical evidence, to be presented later, supports this hypothesis. The failure morphology was indicative of mode II (shear) dominated fracture, parallel to the stringer length. However, there was some evidence of growth in from the edges at the corners of the stringer.

SPEC-2

The results of a single back-to-back strain gauge pair are presented in Fig. 6. The maximum compressive strain measured by SG 1 was significantly less than that measured for SPEC-1 at the corresponding location. The thicker unsupported skin in this region reduced the bending deformation at the edge of the runout. Back-to-Back strain gauge pairs mounted along the flange over the ramped skin section (not shown) exhibited a gradual reduction in bending strain away from the unsupported skin section. Despite the reduced bending energy available for crack propagation, the specimen failed by unstable crack propagation at a loading of 330 kN and corresponding to an end-displacement of 1.29 mm. A video recording of the failure event using a standard 25 frames per second tape speed showed that the crack propagated across the whole interface within a single frame, i.e., within 40 milliseconds.

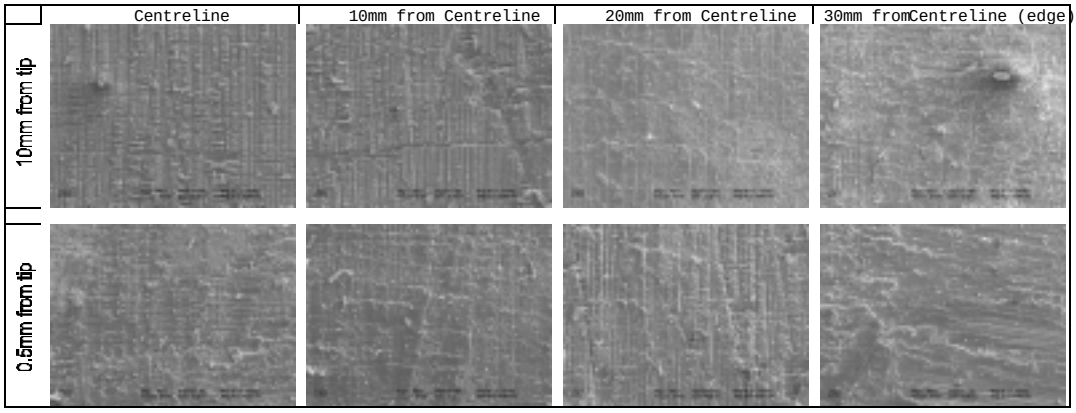

Fig: 5 Fracture surface at skin-stiffener interface (750x, 0° tilt) for SPEC-1 SPEC-3

The strain gauge locations for this specimen are given in Fig. 3. SG 1-SG 2 were placed 15 mm on either side of the centreline and 5 mm away from the end of the runout. This specimen is a scaled up version of SPEC-1 but incorporating a thicker constant skin thickness of 13 mm and a runout region of 400 mm. The maximum measured compressive strain at the end of the runout was 5820 μs. This was measured by a gauge which formed the mirror image, about the centreline, of SG 1 (not shown). The difference in the readings between these two gauges was due to a misalignment of SG 1. SG 3-SG 4 were positioned 5 mm away from the end of the runout along the stiffener and at the same distance from the centreline as SG 1-SG 2. There is very little bending at this location (Fig. 7) and the inner surface (top of stiffener flange, SG 3) actually goes slightly in tension suggesting that a change in curvature occurred close to the end of the runout. SPEC-3 failed at a loading of 538 kN corresponding to an end-displacement of 1.38 mm. The failure of this specimen was characterised by crack initiation and unstable crack propagation followed by stable crack growth. This allowed the test to be stopped, at a loading of 538 kN, before the crack had propagated throughout the whole specimen. This behaviour was in contrast to that of the first set of specimens with a predominantly thinner skin thickness. A summary of the main experimental results is given in Table 3.

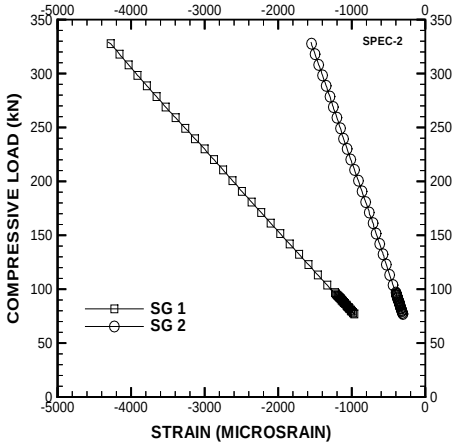

Fig. 6 Strain gauge results for SPEC-2

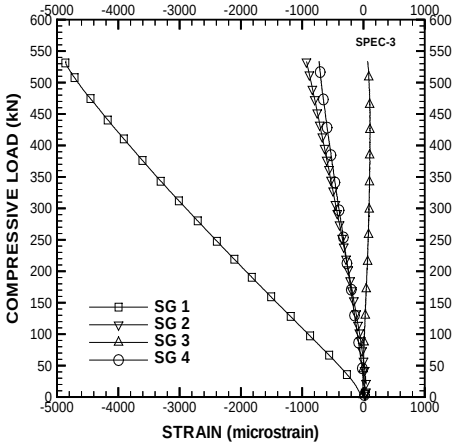

Fig. 7 Strain gauge results for SPEC-3

Table 3 Summary of experimental results

SPECIMEN	FAILURE LOAD (kN)	END-DISPLACMENT (mm)	COMMENTS
SPEC-1	245	1.27	Unstable Crack Growth in 0°/90° interface of closing plies.
SPEC-2	330	1.29	Unstable Crack Growth in skin-closing plies interface.
SPEC-3	538	1.38	Stable crack growth at skin-closing plies interface.

ANALYSIS

FINITE ELMENT MODELLING OF RUNOUT SPECIMENS

A virtual crack closure technique (VCCT) [5-6] was used in the analysis and each runout specimen was modelled using thick shell composite elements [7] developed for the finite element

research code FE77 [8]. The load path eccentricity on the specimen was such as to place the crack surfaces in compression. This implied that the crack propagation mode was predominantly Mode II and calculations involving Modes I and II separation were not deemed necessary. The most computationally efficient way of calculating the strain energy release rate was by noting the change in total strain energy of the local model at a sequence of increasing crack lengths

The modelling of crack growth was made with the assumption that the crack across the width of the stiffener flange was straight and propagated uniformly from the edge of the runout. As the crack propagates it is expected that Mode I will become significant as the unsupported skin may buckle and the problem becomes highly non-linear. The present analysis was limited to the first 20-30 mm of crack length.

FE MODELLING OF SPEC-1

The finite element model for SPEC-1 is shown in Fig. 8(a). The applied end-displacement yielded a load resultant which was offset from the cross-section's neutral plane hence the bending observed in the displaced model shown in Fig. 8(b). It is noted that there is a region of high bending at the edge of the runout which places the skin-stiffener interface in compression. Indeed, it is this bending that provides the energy for crack propagation. High interlaminar shear stresses predicted at the edge of the runout were consistent with the assumption that initial crack propagation was Mode II. High compressive forces at this edge were also evident in the finite element analysis.

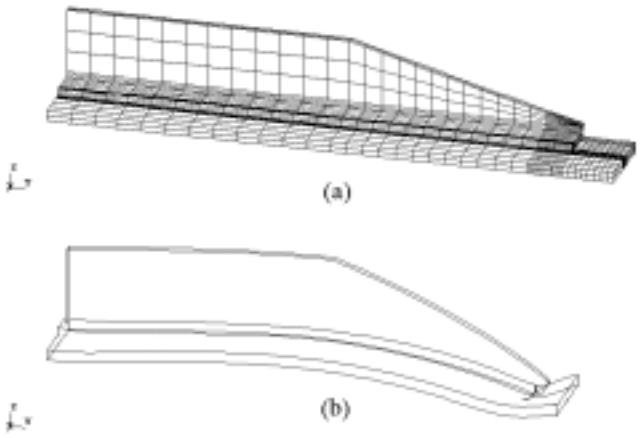

Fig. 8 (a) Finite element model for SPEC-1. (b) Deformed model under compressive loading.

A resistance (or R-) curve, which is a plot of Strain Energy Release Rate (S.E.R.R. or G) versus crack length, for a crack propagating at the skin-stiffener interface is shown in Fig. 9. It is generally assumed that in using this type of analysis, the 'plateau' region of the R-curve represents the value of G to initiate crack propagation. A positive slope on this curve indicates that the crack growth is unstable, that is, the crack will grow with no additional loading. A negative slope indicating that the crack growth is stable and will only propagate with increased loading unless the curve is above a critical value.

Using this assumption for crack propagation, the values of strain energy release rates, S.E.R.R., in the 'plateau' region (where there is a levelling off in the gradient of S.E.R.R. with respect to crack

length) are considerably higher than the quoted co-cured G_{IIC} value for this material (635 J/m^2). As shown earlier, there are high compressive stresses acting in this localised region which may go some way in explaining the disparity between the experimental and analytical results. Qualitatively, the curve shows that the crack is initially highly unstable and the gradient levels off at a crack length of approximately 22 mm. This reduction in crack instability is still occurring at a G value which is above G_{IIC} hence the crack will continue to propagate. This is consistent with experimental observation.

The presence of large compressive stresses at the location of initial failure may delay the onset of fracture although this hypothesis would need further investigation, possibly through the development of an appropriate coupon test. This would also make it possible to quantitatively assess the accuracy of the present finite element analysis. If the R-curve is extrapolated to zero crack length, the critical crack length is approximately 0.86 mm, beyond which, the crack is highly unstable.

FE MODELLING OF SPEC-2

The thick-shell element formulation does not support ply terminations within an element and further assumes that the thickness is constant. To work within this limitation approximations were made in modelling this region. The ramped region was subdivided into thirteen sections with each section representing a ply termination. The lay-up thickness was assumed constant throughout the element and dummy layers were used to get the correct geometric offset of the respective plies. The geometry of the ramp was correctly represented resulting in a slight inconsistency in the way the stiffness matrix is formulated. The volume integral was calculated from the geometry of the section but the elasticity matrix [D] was calculated from the individual plies within the laminate of constant thickness. It should be noted that these approximations are reasonable because of the gentle gradient of this ramped section (1:25).

Fig. 9 shows an R-curve for a crack propagating at the skin-stiffener interface of this specimen. The values of G predicted for this problem were lower than those for Spec-1. This is consistent with the observation made earlier that the bending deformation at the edge of the runout, which provided the energy for crack growth, was reduced due to a thicker skin section in this region. The crack growth is still highly unstable which, again, is consistent with experimental observation. The extrapolated R-curve yielded a critical crack length of 1.5 mm.

FE MODELLING OF SPEC-3

Failure of this thicker-skinned specimen was characterised by initially unstable and then stable crack growth allowing for the test to be terminated before the stiffener had completely disbonded from the skin. The R-curve for this specimen is also shown in Fig. 9. This result is remarkably different from those obtained for the earlier specimens yet fully consistent with experimental observations in that this thick-skinned specimen was characterised by stable crack growth. The critical crack length, from the FE analysis, was calculated at 1.07 mm. The crack then propagated to a length of 20.7 mm where it was observed that the slope of the R-curve is negative and below the critical G_{IIC} value.

In the experiment, the crack propagated to nearly half the length of the specimen as opposed to only 20.7 mm as predicted by analysis. Mention needs to be made of the non-idealised loading conditions on the specimen arising from the finite stiffness of the compression test machine. Added energy may have been provided to the specimen once the crack started to propagate. Dynamic effects have also not been accounted for. The analysis was only performed to a crack

length of 27 mm but even over this length, the slope of the curve was observed to decrease with increasing crack length and may asymptote to some S.E.R.R. value below G_{IIC} for this applied load. Any extra loading provided by the testing machine could bring this curve above the G_{IIC} over a longer crack length.

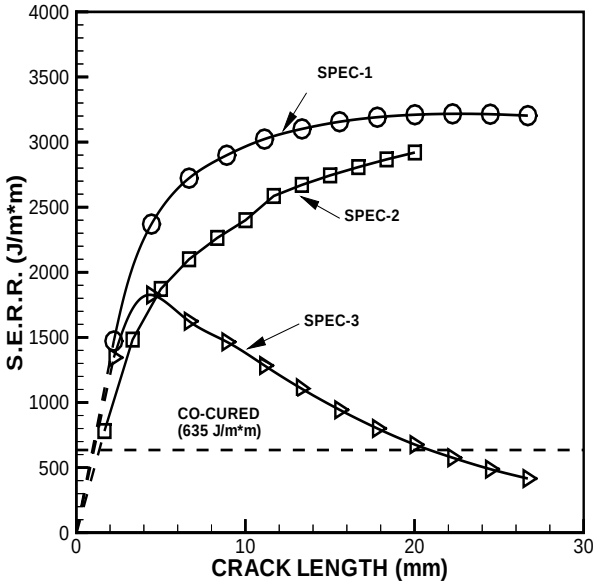

Fig. 9 Strain energy release rate curves.

CONCLUDING REMARKS

A combined experimental and numerical study into the failure of thick-sectioned stiffener runout regions under compression loading was presented. This work was also aimed towards the development of efficient analytical methodologies for the prediction of the failure of thick structural composites which could find use in a design environment. With the imminent launch of the next generation European military transport and the Airbus large capacity civil transport, it became apparent that the potential use of carbon-fibre in the primary structure would highlight the need to be able to better predict debonding of stiffeners in a co-cured stiffened structure. In particular, stiffener termination regions, runouts, were identified as being more susceptible to this mode of failure due to the high interlaminar shear stresses that develop towards the free end of the stiffener.

The experimental results presented in this paper form a subset of a larger series of experiments investigating the failure of stiffener runouts. Failure under compressive loading was shown to be Mode II dominated and a fractographic analysis revealed high through-thickness compression and friction near the edge of the runout. While the first two specimens failed by unstable crack propagation across the whole skin-stiffener interface, the failure of the third specimen was characterised by initially unstable crack growth followed by stable growth.

An efficient thick shell composite element was used for the finite element analysis along with a virtual crack closure technique. The analysis was effective in qualitatively simulating the

behaviour of crack propagation in the three specimens. The large analytical values of strain energy release rates still remains to be resolved satisfactorily although these results do imply an increase in fracture toughness due to the high through-thickness compressive forces at the edge of the runout. The unstable crack propagation in the first two specimens was confirmed analytically. The finite element analysis was also able to show the initial unstable crack growth followed by stable crack propagation for the SPEC-3.

ACKNOWLEDGEMENT

The authors would like to acknowledge the financial support provided under DTI CARAD contract No. DRA/SMC/4/968 and the support of BAe Systems (AIRBUS) in manufacturing the test specimens and Dr Emil Greenhalgh (DERA) for his work on the fractographic analysis.

REFERENCES

1. STEVENS, K.A., RICCI, R., DAVIES, G. A.,O., "Buckling and Postbuckling of Composite Structures", Composites, 26(3), pp 189-199, 1995.
2. FALZON, B. G., STEVENS, K. A., DAVIES, G. A. O., "Postbuckling Behaviour of a Blade-Stiffened Composite Panel Loaded in Uniaxial Compression", Composites Part A: Applied Science and Manufacturing, 31, pp 459-468, 2000.
3. DAVIS, JR., D. D., FARLEY, G. L., AMBUR, D. R., DAVIS, R. C., SHUART, M. J., WANG, J. T., LOTTS., C. G., " An Analytically Designed Subcomponent Test to Reproduce the Failure of a Composite Wing Box Beam", AIAA Conference Paper 93-1344, 1993.
4. BROOKS, W.G., "Load Test Report on Compression Stiffener Runout Panel", BAe Report, April 1995.
5. IRWIN, G.R., "Fracture", Handbuch der Physik **6**, p 588, 1965.
6. RYBICKI, E.F., KANNINEN, M.F., "A Finite Element Calculation of Stress Intensity Factor by a Modified Crack Closure Integral", Engineering Fracture Mechanics **9**, 1977, pp 931-938.
7. FALZON, B. G., HITCHINGS, D., BESANT, T., "Fracture mechanics using a 3D composite element", Composite Structures 45 (1999) pp 29-39.
8. HITCHINGS, D., "FE77 User Manual", Imperial College of Science, Technology & Medicine, 1994.